

A Modified Design Approach for Compact Ultra-Wideband Microstrip Filters

Marjan Mokhtaari,¹ Jens Bornemann,¹ Smain Amari²

¹ Department of Electrical and Computer Engineering, University of Victoria, Victoria, BC, Canada V8W 3P6

² Department of Electrical and Computer Engineering, Royal Military College of Canada, Kingston, ON, Canada K7K 7B4

Received 26 May 2009; accepted 12 August 2009

ABSTRACT: A modified design approach for compact ultra-wideband microstrip filters with cascaded/folded stepped-impedance resonators is described. The key feature of the proposed method is to facilitate stronger coupling between stepped-impedance resonators and, at the same time, eliminate the requirement of extremely small gaps in coupled-line sections, as found in traditional designs. Simulations and measurements demonstrate that the filters designed with this technique exhibit good reflection, insertion-loss, and group-delay performance within the 3.1–10.6 GHz band. © 2009 Wiley Periodicals, Inc. *Int J RF and Microwave CAE* 20: 66–75, 2010.

Keywords: ultra-wideband filters; filter synthesis; stepped-impedance resonator; microstrip filter; coupling segments

I. INTRODUCTION

Since the introduction of the unlicensed use of ultra-wideband technology in the 3.1–10.6 GHz range, the realization of low-cost ultra-wideband wireless systems has been considered a priority for both military and commercial applications [1]. In this context, the characterization, design, and fabrication of bandpass filters covering an ultra-wideband frequency range have been the challenging tasks (e.g., as shown in Refs. 2–5). To minimize distortions of the ultra-wideband signal, it is essential to maintain filter linearity (amplitude and group delay) within the passband and good selectivity and suppression in the stopband.

Recent ultra-wideband filter designs tend to focus on compactness for reasons of fabrication, cost, and integration with other systems [6–24]. Conventional configurations of the stepped-impedance resonator (SIR) and traditional microstrip filter designs require very small gaps between the coupled segments, hence resulting in high manufacturing accuracy, and thus, higher expenses [9–17].

Although a single microstrip stepped-impedance resonator, which is tightly coupled to the input/output lines, is

capable of producing an ultra-wideband filter covering the 3.1–10.6 GHz frequency range, its attenuation on both sides of the passband is rather poor [6, 9]. On the other hand, cascading multiple stepped-impedance resonators features good performance in both passband and stopband regions, but the designs require rather long, thus spacious areas on printed-circuit boards [25, 26].

In the past few years, several planar filter configurations have been reported for ultra-wideband applications. However, issues such as reducing size and manufacturing cost and simultaneously enhancing performance have not necessarily been priorities in ultra-wideband filter designs.

Therefore, the purpose of this work is to introduce a modified design approach by using stepped-impedance resonators, which facilitate stronger coupling between filter elements and input/output ports. Thus, the traditional requirement of relatively small gaps in coupled-line sections is eliminated. In this context, a new and compact stepped-impedance resonator composed of parallel high-impedance and folded low-impedance segments, which differs from the dual-band applications in [27, 28], is presented and utilized in the design of ultra-wideband filters with and without source/load coupling. Measurements and/or results obtained with commercially available field solvers verify all designs.

Correspondence to: M. Mokhtaari; e-mail: marjan@uvic.ca
DOI 10.1002/mmce.20407

Published online 10 November 2009 in Wiley InterScience (www.interscience.wiley.com).

II. TRADITIONAL DESIGN

To highlight our design approach as outlined in Section III, we begin with shortly describing the traditional design of UWB microstrip filters.

Assume that we want to design an ultra-wideband filter covering the frequency range from 3.1 GHz to 10.6 GHz. The midband frequency is located at 6.85 GHz with a fractional bandwidth of 110%. The design procedure is based on a Chebyshev bandpass filter synthesis with 50 Ω input/output impedances and at least 12 dB return loss within the passband. Traditionally, this filter can be modeled by an eleven-pole ($N = 11$) shunt-stub prototype where the stubs are separated by quarter-wavelength admittance inverters as shown at the top of Figure 1a. All impedance values are in ohms, and C/L denotes the centerline of the symmetric filter structure. The element values are extracted from Chebyshev low-pass filter coefficients [29, 30]. The duality of this filter using series open-circuited stubs (Fig. 1a, center) is obtained through direct synthesis in dual form. Kuroda's identities (or capacitance matrix transformation) provide the edge-coupled sections separated by double equal-value unit elements (Fig. 1a, bottom). This procedure simply transforms the model to a quarter-wavelength coupled-section configuration [29, 30], which effectively resembles the stepped-impedance passband filter structure shown in Figure 1b. Its response, based solely on impedance values and electrical line lengths and excluding fringing fields, etc., is shown in Figure 1c as Cascaded Transmission Line (CTL) theory (dashed lines).

To fabricate this filter in microstrip technology, we specify a substrate; for instance RT6006, $\epsilon_r = 6.15$, substrate thickness = 635 μm, conductor thickness = 17 μm. The next step is to translate the impedance parameters and line lengths from Figure 1b to actual circuit dimensions. This is accomplished by using standard references with closed-form expressions for a variety of quantities. The reader is referred to Ref. 31, which contain all expressions used in this work.

Because of the strong coupling coefficients $k_1 = 0.65$ and $k_2 = 0.58$ for the first/last and middle coupling sections, respectively, between quarter-wavelength high-impedance segments (as obtained from the prototype Chebyshev synthesis), very small gaps of 10 μm and 40 μm between the coupled lines are required to cover the entire band. One half of the circuit layout (including dimensions in mm), is shown in the inset of Figure 1c. Such narrow gaps between coupled lines are prohibitive when low-cost, mass-producible manufacturing is envisaged.

Moreover, the full-wave simulations in Figure 1c show a 3 dB bandwidth from 3.15 GHz to 10.15 GHz, which is 8% smaller than the bandwidth computed from CTL theory. In addition, the two full-wave simulations reveal a resonance peak at around 13 GHz which is not produced by the simple CTL theory. This peak is related to the fourth harmonic response of the implemented stepped-impedance resonators as will be discussed in the next section.

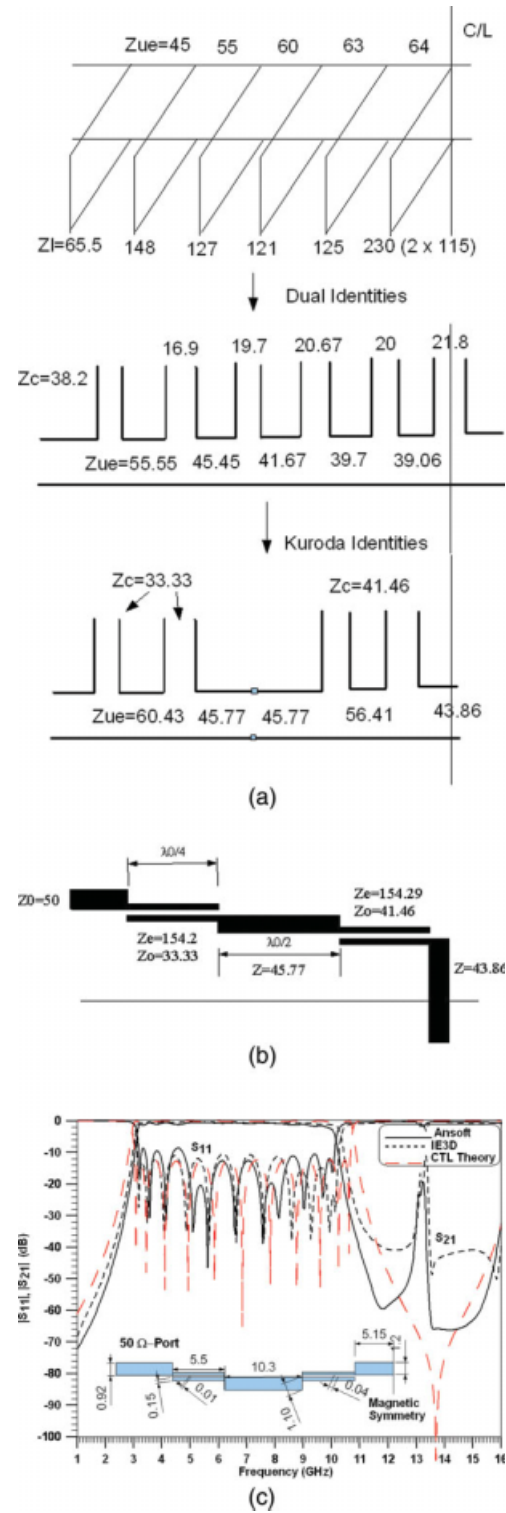


Figure 1 Traditional UWB microstrip filter design procedure; design steps (a), impedance parameters (b), comparison of filter performances using transmission-line theory and two full-wave solvers (c). Note that only one half of the symmetric filter structures are shown; all impedances are in ohms, all dimensions in millimeters. [Color figure can be viewed in the online issue, which is available at www.interscience.wiley.com.]

III. MODIFIED DESIGN

Besides the reduction in bandwidth, which can be compensated for by targeting for a slightly wider band, the main concerns with the traditional design are the narrow gaps between lines and the higher-order resonances of the stepped-impedance resonators. We will address the last item first and will alleviate the gap-width requirement by introducing a different stepped-impedance resonator. However, we will come back to the possibility of so-called interdigital coupling at the end of this section.

It is obvious from the full-wave results in Figure 1c that higher-order resonances of the stepped-impedance resonator influence the UWB filter performance. Therefore, we start with analyzing the resonances of a stepped-impedance resonator.

A. Design Guidelines

Figure 2a shows a schematic view of the stepped-impedance resonators used for our practical designs. They include a structure with folded low-impedance (Z_1) and parallel high-impedance segments (Z_2). The main task in using a stepped-impedance resonator is to control the harmonic resonance frequencies in terms of the impedance ratio ($R_Z = Z_2/Z_1$) as well as the electrical lengths, $2\theta_1$ and θ_2 , of the low- and high-impedance segments, respectively. This is usually done by solving two transcendental equations for the alternating odd- and even-mode (quasi-TEM) resonances (e.g., as shown in Ref. 8). Figure 1b shows the ratio of the higher-order resonance frequencies to that of the fundamental mode versus the ratio $U = \theta_1/(\theta_1 + \theta_2)$ of electrical lengths (c.f., Fig. 2a) and impedance ratio R_Z as parameter.

In the synthesis of an ultra-wideband filter, the fundamental resonance and a proper number of harmonic resonances must be allocated within the passband. For instance, an ultra-wideband filter utilizing triple-mode stepped-impedance resonators is designed such that the center frequency of the filter is selected to be the first harmonic frequency. This is the arithmetic mean of the fundamental and second harmonic resonances, i.e., $f_2 = \sqrt{f_1 f_3}$, which are properly defined close to the edges of the passband. To cover a specific bandwidth, a number of stepped-impedance resonators should be cascaded and the input/output connected by quarter-wavelength coupled-line sections at the center frequency (θ_2). Note that such sections act as inverters and can increase the order of the ultra-wideband filter by two (e.g., as shown in Ref. 6). The basic concept in the modified UWB filter design is to match the resonant frequencies of the stepped-impedance resonators with the reflection zeros generated from a Chebyshev polynomial [29, 30].

The other parameters of the stepped-impedance resonators can be determined by using the graph in Figure 2b. The value of the electrical length and impedance ratios are selected such that other higher-order modes, which are not utilized in the passband of an ultra-wideband filter, are located as far as possible from the upper edge of the passband. For instance, the points labeled A_1 , B_1 , C_1 , and D_1 in Figure 2b show the locations of different electrical

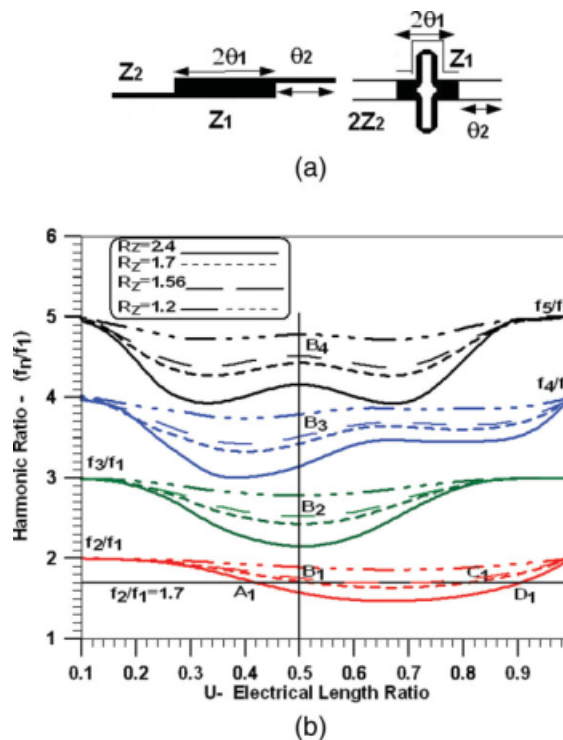


Figure 2 Stepped-impedance resonators used in this work (a), and harmonic ratios of the stepped-impedance resonators in terms of electrical length and impedance ratios (b). [Color figure can be viewed in the online issue, which is available at www.interscience.wiley.com.]

length ratios in terms of various impedance ratios for a specific passband filter design. If the first harmonic ratio placed within the passband is 1.7 for $U = 0.5$ and $R_Z = 1.56$ (B_1), then points B_2 , B_3 , and B_4 represent the locations of the next harmonic frequencies.

Using the first two higher resonances (f_2 and f_3) in addition to the fundamental mode (f_1), the locations of points B_3 and B_4 for the fourth and fifth harmonic frequency ratios should have maximum distance from points B_1 and B_2 to create a wide upper stopband. The larger this band gap, the broader is the upper-band suppression region and the fewer are the effects of those higher-order modes on the main passband performance.

Let us now come back to the example in Section II. According to Figure 1b, the impedance of the first/last coupled segments is calculated as $Z_h = \sqrt{Z_{0c} Z_{0o}} = \sqrt{154.2 \Omega \cdot 33.33 \Omega} = 71.69 \Omega$. Therefore, the impedance ratio of the high- to low-impedance segments is $R_Z = Z_h/Z_1 = 71.69/45.77 = 1.56$. The electrical length ratio is selected as $U = 0.5$ (vertical line in Fig. 2b). Similarly, the impedance ratio of the middle coupled segments is $R_Z = \sqrt{154.29 \Omega \cdot 41.46 \Omega}/43.86 \Omega = 1.82$.

From the graph shown in Figure 2b, the fourth harmonic ratio for the first/last coupled stepped-impedance resonators is $f_4/f_1 = 3.5$, which is equal to the fourth harmonic resonance frequency at 13.65 GHz. The fourth harmonic for the middle stepped-impedance resonator is

similarly calculated as 13.1 GHz. Because of all open-end effects in the full-wave field solvers, the electrical length ratio turns out slightly smaller than 0.5, resulting in a shift of the fourth harmonic resonance from 13.1 GHz to 13.5 GHz (refer Fig. 1c). From the graph in Figure 2b, the fifth harmonic response occurs at 17.16 GHz ($f_5/f_1 = 4.4$ for the middle stepped-impedance resonator when $R_Z = 1.82$ and $U = 0.5$). This additional resonance peak is indicated by the increase in slopes at the right-hand limit of Figure 1c. The transmission zero at 13.7 GHz in Figure 1c is due to the first harmonic response of open-ended coupling segments, which are selected as a quarter-wavelength at mid-band frequency ($f_0 = 6.85$ GHz).

The design can now be modified to create stronger coupling (or larger gap width for given coupling) by introducing two parallel open-ended high-impedance segments at the sides of the first/last stepped-impedance resonators (c.f., Fig. 2a, right). This means that the coupling coefficients remain as before, but the high- and low-impedance segments are scaled. This will change the input/output impedance and introduces a scaled filter synthesis. Therefore, a proper even/odd impedance characteristic is selected for the high-impedance segment, which is connected and matched to the input/output 50 Ω transmission lines.

To find the scale factor over the impedances of transmission lines, we adhere to the following approach.

a. Define the coupling coefficients of coupling segments in terms of even/odd impedance characteristics. Since we introduce three asymmetrically coupled transmission lines for each coupling segment (sometimes also referred to as interdigital coupling topology), the coupling coefficient definition is more complicated [31] than that of two symmetrically coupled transmission lines.

b. The impedance of the input/output coupling segment is selected as 50 Ω to match the connected transmission lines. Thus $Z = \sqrt{Z_{in-e}Z_{in-o}} = \sqrt{Z_{out-e}Z_{out-o}} = 50 \Omega$.

c. The impedance of the parallel high-impedance segments on the sides of the first/last stepped-impedance resonators is selected to have a maximum value of 100 Ω , which prevents line segments from being too narrow. (Note that this value can be changed depending on the substrate and fabrication technique used). Thus, we have $Z_h = \sqrt{Z_{he}Z_{ho}} = 100 \Omega$. Due to two parallel high-impedance segments on the sides of the first and last stepped-impedance resonators, the final high-impedance characteristic will be 50 Ω .

From the above conditions, we have four equations and four variables including Z_{in-o} , Z_{in-e} (Z_{out-o} , Z_{out-e}), Z_{ho} , and Z_{he} . These odd/even impedance characteristics can be approximately calculated by optimization techniques in Matlab. The design parameters in terms of dimensions of asymmetric coupling segments are then calculated from closed-form expressions (e.g., as shown in Ref. 31), for given substrate parameters.

d. The scale factor is defined by the ratio of the first/last high impedance segment value of the Chebyshev synthesis to that calculated from previous steps. Referring to the result of the filter in Figure 9, which will be compared to the design in Figure 1, the scale factor is obtained as

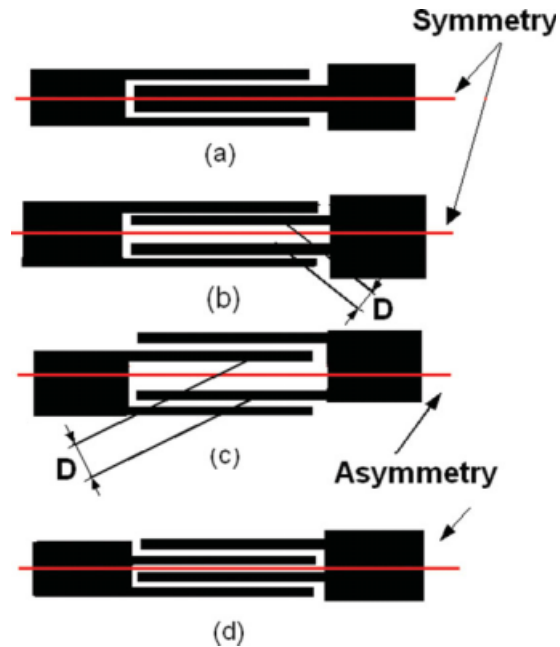


Figure 3 Coupling configurations between cascaded resonators; symmetric coupling segments (a,b), asymmetric coupling segments (c,d). [Color figure can be viewed in the online issue, which is available at www.interscience.wiley.com.]

1.5. This scale factor is used to scale all impedance values of the stepped-impedance resonators.

e. The odd/even high impedance of the center stepped-impedance resonator is also calculated by achieving the proper coupling coefficient from the Chebyshev synthesis on the proposed coupling segment topology (c.f., Fig. 3) and the scale factor calculated from the previous step. Since scaling is applied to all impedances of the stepped impedance resonators, the harmonic ratios remain unchanged.

B. Coupling Between Stepped-Impedance Resonators

To extend the filter bandwidth, multiple cascaded resonators are used. Figure 3 shows symmetric (Figs. 3a and 3b) and asymmetric (Figs. 3c and 3d) coupling scenarios between step-impedance resonators. These configurations appear to be able to generate stronger coupling and, therefore, seem to represent alternative coupling segment compared to the parallel-coupled lines in the inset of Figure 1c.

On closer inspection, though, this is not necessarily the case. Although the scheme in Figure 3a achieves strong coupling with reasonably wide gaps (slots) between the lines, the configurations in Figures 3b and 3c achieve the same coupling only if the center gap D is large enough to separate the two individual couplings of the upper and lower pair. This in turn results in narrower gaps (which are still larger than required from the Chebyshev filter synthesis in the inset of Fig. 1c), and thus, slightly increases accuracy requirements. An example is shown in Figure 4 where the first/last coupling section is according

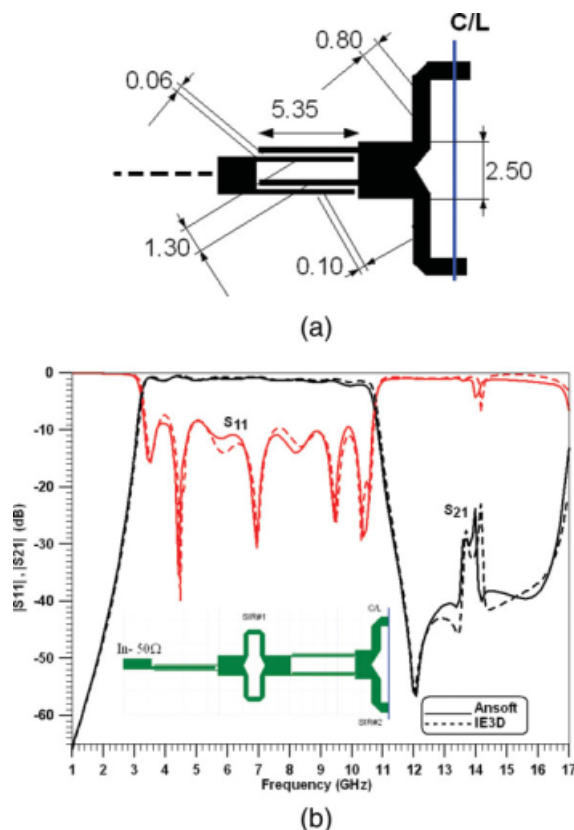


Figure 4 Computed performances of an UWB filter with three stepped-impedance resonators (SIRs) using coupling sections according to Figures 3a and 3c; detailed layout (dimensions in mm) of the coupling sections for the center SIR (a), filter performance using two different full-wave solvers (b). [Color figure can be viewed in the online issue, which is available at www.interscience.wiley.com.]

to Figure 3a and the two center ones according to Figure 3c. (Note that only one half of the filter is shown in the inset of Fig. 4b). As shown in Figure 4a, the minimum gap between coupled lines is $60 \mu\text{m}$ as opposed to $40 \mu\text{m}$ in the Chebyshev synthesis.

For direct comparison, Figure 5 shows the same filter with Figure 3d as center coupling sections (Fig. 5a), which represent so-called interdigital high-impedance coupling segments. Indeed, the achievable couplings with these sections are strong and, therefore, the required coupling coefficients are easily implemented. However, since the two parallel coupling sections (two arms each in Figs. 3b and 3c) are no longer separated in Figure 3d, they couple to each other, and thus, produce two attenuation poles (transmission zeros) symmetrically located on either side of the center frequency. They are shown at 6.6 GHz and 7.4 GHz in Figure 5b.

Therefore, the proposed coupling scheme in Figure 3d might be a suitable solution in triple-band filter applications. Within the scope of this work on UWB filters, however, we will employ the coupling scheme of Figure 3a and standard coupled transmission lines.

IV. RESULTS

This section presents examples of compact ultra-wideband microstrip filters using the design guidelines outlined in Section III(A). All prototypes are fabricated on RT6006 substrate with thickness of $635 \mu\text{m}$ and conductor layers of $35 \mu\text{m}$. The relative permittivity of the substrate is taken as 6.15 for all designs. The final designs have been computed with Ansoft Designer®, verified by IE3D®, then prototyped and measured.

An UWB filter to cover the entire 3.1–10.6 GHz band is designed using three cascaded stepped-impedance resonators in a folded configuration. Figure 6a depicts the filter layout with minimum gap widths of $25 \mu\text{m}$. Simulated and measured filter performances are shown in Figure 6b. The 3 dB fractional bandwidth is 104%. The upper stop-band extends from 10 GHz to 15 GHz with better than 20 dB measured suppression. The insertion loss is less than 2 dB. The substrate size is $28 \text{ mm} \times 15 \text{ mm}$.

Agreement between measurements and simulations is generally good, thus verifying the design procedure. However, a slight downward frequency shift is observed in the measurements (and in those of the following examples). This is attributed to a slightly higher substrate permittivity

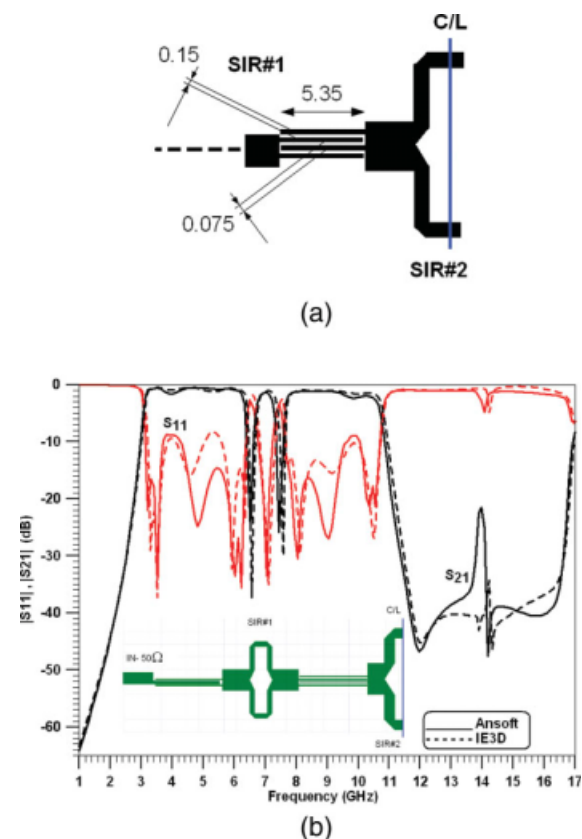


Figure 5 Computed performances of the ultra-wideband filter in Figure 4, but using the coupling schemes of Figures 3a and 3d; detailed layout (dimensions in mm) of the coupling sections for the center SIR (a), filter performance using two different full-wave solvers (b). [Color figure can be viewed in the online issue, which is available at www.interscience.wiley.com.]

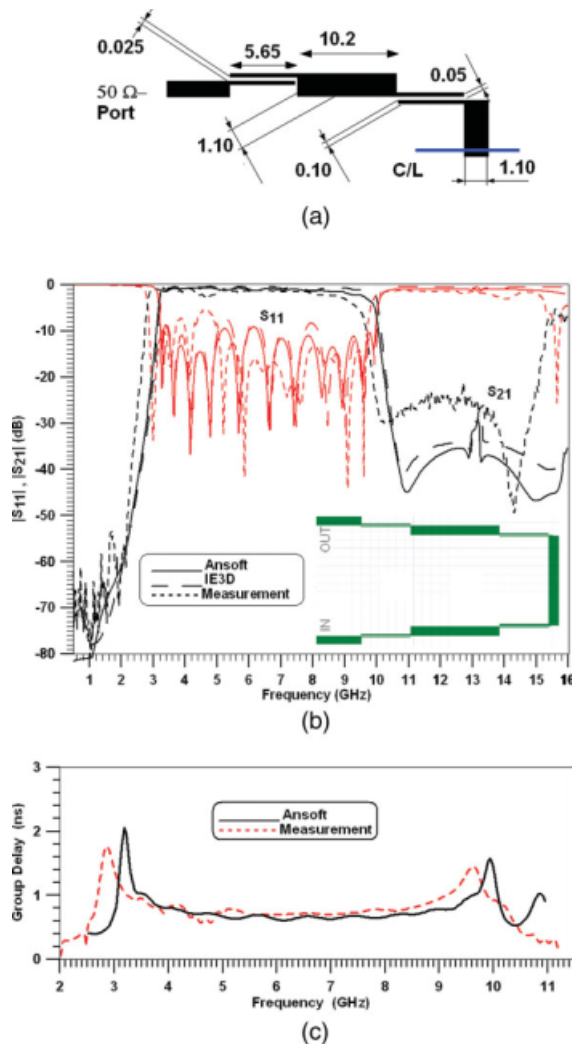


Figure 6 Layout, measured and computed performances of a folded ultra-wideband microstrip filter with three cascaded stepped-impedance resonators and standard coupled transmission lines; dimensions of filter half in millimeters (a), transmission and reflection coefficients in dB (b), group delay (c). [Color figure can be viewed in the online issue, which is available at www.interscience.wiley.com.]

and metal-etching tolerances. (The reader is referred to [32] for a discussion on tolerances). The appearance of the transmission minima in the upper stopband is due to the inter-coupling between the harmonic and fundamental quasi-TEM resonances. Note that due to the complexity of the stepped-impedance resonator for triple-mode resonance operation, a direct coupling-matrix-type model (typically used for narrowband filters) has very limited validity in UWB applications because of the frequency dependency of coupling elements and coefficients.

Figure 6c shows the measured and computed group delay performance of the filter, which is extracted from the transmission phase computations and measurements in the passband as $\tau = -\partial\varphi_{21}/\partial\omega$. In or close to the stopband(s), the output signal is diminished due to high

attenuation and the existence of attenuation poles. Therefore, in stopband frequency ranges very close to the passband, we use the phase properties of lossless symmetrical two-port devices and extract the group delay from the phase of the reflection coefficient S_{11} : $\varphi_{11} = \varphi_{21} \pm \pi/2$. The group delay is meaningless at stopband frequencies far away from the passband and, therefore, Figure 6c (and following group delay plots) focus mainly on the ultra-wide passband. The results in Figure 6c demonstrate that the group delay variation in the passband is less than 0.4 ns and that good agreement between experimental and numerical results is obtained.

In some applications, sharper transitions from the passband to the stopbands are required. The implementation of source/load coupling supports such an approach by allocating attenuation poles on both sides of the passband. The locations of the attenuation poles are defined in terms of the sign and the strength of the source/load coupling.

The layout and performance of the ultra-wideband filter of Figure 6, but with added source/load coupling, is depicted in Figure 7. A source/load coupling is maintained through phase difference computation between transmission signals of the input of the first stepped-impedance resonator (SIR) and the output of the last SIR at center frequency. This phase difference should be 180° , which determines the distance of transmission lines from the input and output of the first and last SIRs, respectively (c.f., Fig. 7a). The substrate size is 32 mm \times 23 mm. Six attenuation poles at 1.4 GHz, 3 GHz, 10.2 GHz, 12 GHz, 14 GHz, and 16 GHz are generated through the positive source/load coupling (Fig. 7b). Except for the frequency shift mentioned earlier, these poles are well represented in the measurements, and overall agreement is good. However, as a direct result of source/load coupling, the overall stopband attenuation level in Figure 7b is lower than that of Figure 6b.

The filter performance demonstrates that not necessarily all of the theoretical maximum number of transmission zeros (according to traditional filter theory) can be independently placed. This is due to the fact that the coupling between resonances in individual stepped-impedance resonators does not follow the traditional coupling scheme, which assumes constant coupling between resonators.

Figure 7c reports the numerical and experimental group delay results. Compared to Figure 6c, the variation is increased to 0.6 ns.

Figure 8 shows the layout and performance of a five-pole UWB microstrip filter using a single triple-mode stepped-impedance resonator with folded low-impedance and parallel high-impedance segments (c.f., Fig. 2a, right). Input and output ports of the stepped-impedance resonator are folded to permit source/load-coupling implementation. The substrate size of the prototype is only 17 mm \times 20 mm with dimensions given in Figure 8a. The minimum gap width is 0.1 mm. The symmetrical source/load coupling is positive and generates two attenuation poles on each side of the passband at 1.8 GHz, 2.4 GHz, 8.8 GHz, and 9.6 GHz (Fig. 8b). As seen in the previous example, source/load coupling lowers the attenuation level in the

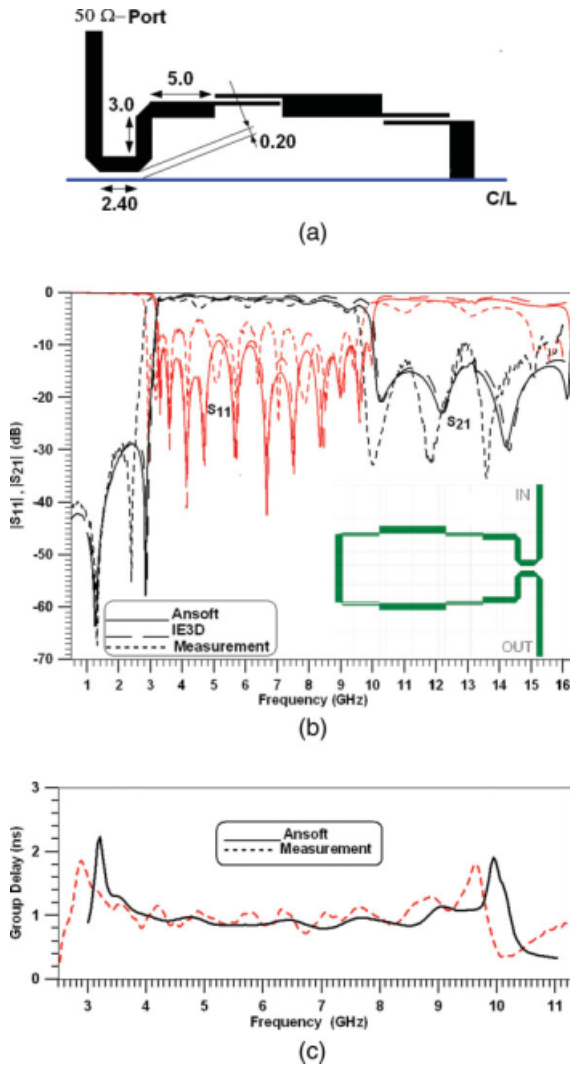


Figure 7 Filter structure, measured and computed performances of the folded ultra-wideband filter in Figure 6, but with added source/load coupling; added dimensions (compared to Fig. 6a) in millimeters (a), transmission and reflection coefficients in dB (b), group delay (c). [Color figure can be viewed in the online issue, which is available at www.interscience.wiley.com.]

stopband (Fig. 8b) and increases group delay variations (Fig. 8c).

To demonstrate that the modified design approach of Section III(A) leads to wider gap widths and more compact filter components, we finally return to the design presented in Section II. In comparison with Figure 1c, three cascaded triple-mode stepped-impedance resonators with folded low-impedance and parallel high-impedance segments are used to design an eleven-pole UWB microstrip filter on a substrate size of 45 mm × 8 mm. (Note that the size of the substrate in the inset of Fig. 1c is narrower but longer: 63 mm × 4 mm.)

A comparison between both filter structures in Figures 1c and 9a reveals that much larger gaps are achieved (40 μm and 85 μm in Fig. 9a compared to 10 μm and 40 μm ,

respectively, in Fig. 1c) by using our alternative design approach. Figure 9b shows the numerical and experimental performances. From the graph in Figure 2b, the fourth harmonic responses of the two different stepped-impedance resonators occur at 13.5 GHz and 14 GHz which are seen in Figure 9b at around 14 GHz. Because of asymmetric coupling configurations, the transmission zero at 13.7 GHz in Figure 1c moves down to 12 GHz in Figure 9b to create a sharper passband-to-stopband transition. The performance in Figure 9b demonstrates that the filter covers a bandwidth between 3 GHz and 10.7 GHz. (Note that the two wider dips in the S_{11} performance resemble two reflection zeros each; but the theoretical fine-tuning of the filter was terminated once a return loss of 10 dB had been achieved.) Good agreement between the

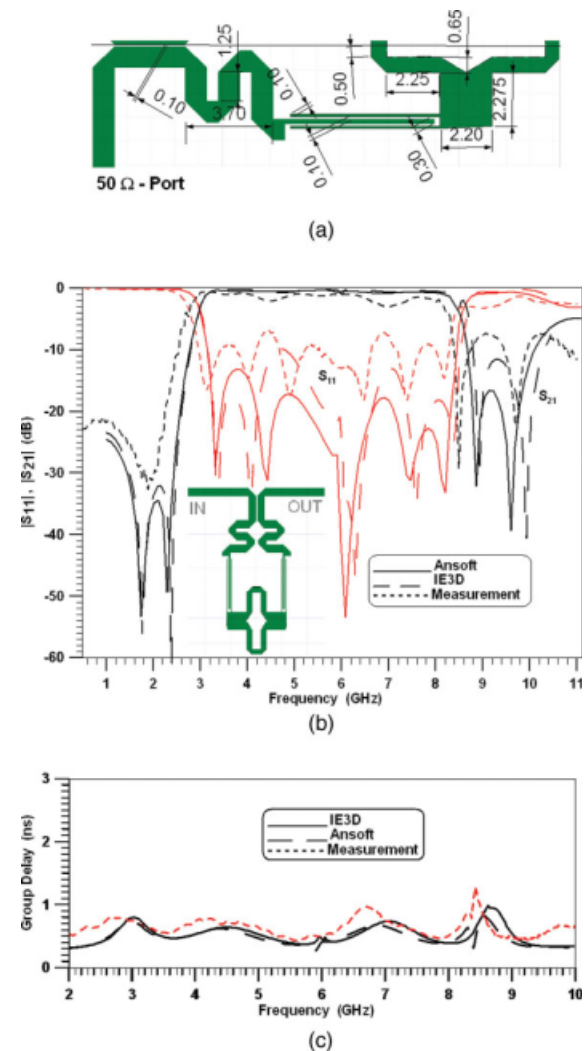


Figure 8 Measured and computed performances of a five-pole ultra-wideband filter with a single triple-mode stepped-impedance resonator with folded low-impedance and parallel high-impedance segments and added source/load coupling; dimensions of one filter half in millimeters (a), transmission and reflection coefficients in dB (b), group delay (c). [Color figure can be viewed in the online issue, which is available at www.interscience.wiley.com.]

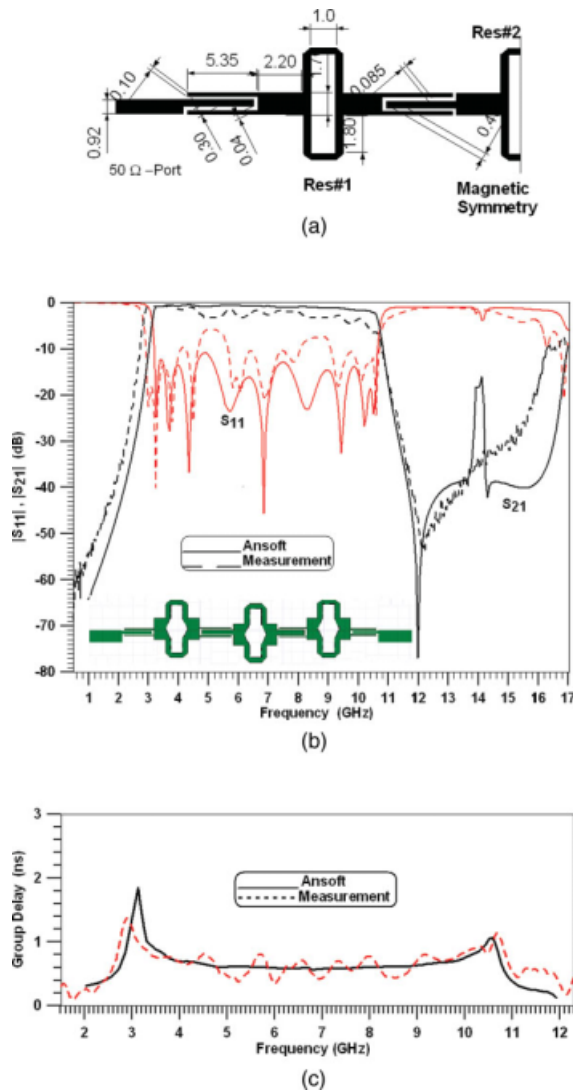


Figure 9 Measured and computed performances of an eleven-pole UWB microstrip filter with three cascaded triple-mode stepped-impedance resonators and folded low-impedance and parallel high-impedance segments for comparison with Figure 1; dimensions of one filter half in millimeters (a), transmission and reflection coefficients in dB (b), group delay (c). [Color figure can be viewed in the online issue, which is available at www.interscience.wiley.com.]

numerical and experimental results is observed. Especially, the steep slope between 11 GHz and 12 GHz is reproduced by the measurements. However, the peak in the S_{21} performance at 14 GHz is not. This is attributed to slightly stronger coupling (slightly narrower gap in the prototype) between the cascaded stepped-impedance resonators. Note that the bandwidth is also slightly increased due to this effect. Figure 9c depicts the group delay performance of both simulation and experiment. The measured group delay variation is roughly 0.7 ns within the band of interest.

V. CONCLUSIONS

The modified design approach for ultra-wideband microstrip filters, in combination with a compact stepped-impedance resonator composed of parallel high-impedance and folded low-impedance segments, eliminates the extremely narrow coupling gaps known from traditional designs. It is shown that for a comparable filter, the smallest coupling gaps can be four times larger than in traditional designs. Therefore, the resulting filters are more amenable to low-cost fabrication techniques despite being reasonably small due to the type of stepped-impedance resonator used. The reported numerical and experimental results demonstrate the feasibility of the design process. To improve filter selectivity, source/load coupling can be added to create attenuation poles left and right of the passband. However, this measure has proven to be a disadvantage when low group-delay variations and high stop-band levels are envisaged.

ACKNOWLEDGMENTS

This work was supported by the Natural Sciences and Engineering Research Council of Canada, and the TELUS Research Grant in Wireless Communications.

REFERENCES

1. Federal Communications Commission (FCC), Revision of part 15 of the commission's rules regarding ultra-wideband transmission systems, First Report and Order, FCC 02-48, 2002.
2. H.J. Carlin and W. Kohler, Direct synthesis of band-pass transmission line structures, *IEEE Trans Microwave Theory Tech* 13 (1965), 283–297.
3. M.C. Horton and R.J. Wenzel, General theory and design of optimum quarter-wave TEM filters, *IEEE Trans Microwave Theory Tech* 13 (1965), 316–327.
4. R.J. Wenzel, Exact theory of interdigital band-pass filters and related coupled structures, *IEEE Trans Microwave Theory Tech* 13 (1965), 559–575.
5. Z.N. Chen, X.H. Wu, H.F. Li, N. Yang, and M.Y.W. Chia, Considerations for source pulses and antennas in UWB radio systems, *IEEE Trans Antennas Propag* 52 (2004), 1739–1748.
6. L. Zhu, S. Sun, and W. Menzel, Ultra-wideband bandpass filters using multiple-mode resonator, *IEEE Microwave Wireless Comp Lett* 15 (2005), 796–798.
7. M. Mokhtaari, J. Bornemann, and S. Amari, Compact planar ultra-wide pass-band filters with source-load coupling and impedance stubs, 2006 Asia-Pacific Microwave Conf, Yokohama, Dec. 2006, pp. 155–158.
8. M. Mokhtaari, J. Bornemann, and S. Amari, Folded compact ultra-wideband stepped-impedance resonator filters, 2007 IEEE MTT-S Int. Microwave Symp, Honolulu, June 2007, pp. 747–750.
9. W. Menzel, L. Zhu, K. Wu, and F. Bogelsack, On the design of novel compact broadband planar filters, *IEEE Trans Microwave Theory Tech* 51 (2003), 364–370.
10. H. Wang, L. Zhu, and W. Menzel, Ultra-wideband bandpass filter with hybrid microstrip/CPW structure, *IEEE Microwave Wireless Comp Lett* 15 (2005), 844–848.
11. S. Sun and L. Zhu, Capacitive-ended interdigital coupled lines for UWB bandpass filters with improved out of band performances, *IEEE Microwave Wireless Comp Lett* 16 (2006), 440–442.

12. R. Li and L. Zhu, Compact UWB bandpass filter using stub-loaded multiple-mode resonator, *IEEE Microwave Wireless Comp Lett* 17 (2007), 40–42.
13. S.W. Wong and L. Zhu, EBG-embedded multiple-mode resonator for UWB bandpass filter with improved upper-stopband performance, *IEEE Microwave Wireless Comp Lett* 17 (2007), 421–423.
14. S. Sun and L. Zhu, Wideband microstrip ring resonator bandpass filters under multiple resonances, *IEEE Trans Microwave Theory Tech* 55 (2007), 2176–2182.
15. S.W. Wong and L. Zhu, Implementation of compact UWB bandpass filter with a notch-band, *IEEE Microwave Wireless Comp Lett* 18 (2008), 10–12.
16. K. Li, UWB bandpass filter: Structure, performance and application to UWB pulse generation, 2005 Asia-Pacific Microwave Conf, Suzhou, Dec. 2005, pp. 79–82.
17. J. Gao, L. Zhu, W. Menzel, and F. Bogelsack, Short-circuited CPW multiple-mode resonator for UWB bandpass filter, *IEEE Microwave Wireless Comp Lett* 16 (2006), 104–106.
18. W. Menzel and P. Feil, Ultra-wideband (UWB) filter with WLAN notch, 2006 European Microwave Conf., Manchester, Sep. 2006, pp. 595–598.
19. H. Shaman and J.-S. Hong, Ultra-wideband (UWB) bandpass filter with embedded band notch structures, *IEEE Microwave Wireless Comp Lett* 17 (2007), 193–195.
20. H. Shaman and J.-S. Hong, Asymmetric parallel-coupled lines for notch implementation in UWB filters, *IEEE Microwave Wireless Comp Lett* 17 (2007), 516–518.
21. S.W. Wong and L. Zhu, Implementation of compact UWB bandpass filter with a notch-band, *IEEE Microwave Wireless Comp Lett* 18 (2008), 10–12.
22. G.-M. Yang, R. Jin, C. Vittoria, V.G. Harris, and N.X. Sun, Small ultra-wideband (UWB) bandpass filter with notched band, *IEEE Microwave Wireless Comp Lett* 18 (2008), 176–178.
23. K. Li, D. Kurita, and T. Matsui, UWB bandpass filters with multi notched bands, 2006 European Microwave Conf., Manchester, Sep. 2006, pp. 591–594.
24. S. Sun and L. Zhu, Multiple-resonator-based bandpass filters, *IEEE Microwave Mag* 10 (2009), 88–98.
25. Y.-C. Chiou, J.-T. Kuo, and E. Chang, Broadband quasi-Chebyshev bandpass filter with multimode stepped-impedance resonators (SIR's), *IEEE Trans Microwave Theory Tech* 54 (2006), 3352–3358.
26. K. Li, D. Kurita, and T. Matsui, Dual-band ultra-wideband bandpass filter, 2007 IEEE MTT-S Int. Microwave Symp, Honolulu, June 2007, pp. 1193–1196.
27. M. Mokhtaari, J. Bornemann, and S. Amari, Quasi-elliptical dual-band stepped-impedance filters with folded parallel high-impedance segments, 2007 European Microwave Conf, Munich, Oct. 2007, pp. 862–865.
28. M. Mokhtaari, J. Bornemann, and S. Amari, Dual-band stepped-impedance filters for ultra-wideband applications, 2007 European Microwave Conf, Munich, Oct. 2007, pp. 779–782.
29. G.L. Matthaei, L. Young, and E.M.T. Jones, *Microwave filters, impedance-matching networks and coupling structures*, Artech House, Dedham, 1980.
30. D.M. Pozar, *Microwave engineering*, John Wiley & Sons, New York, 2005.
31. B.C. Waddell, *Transmission line design handbook*, Artech House, Boston, 1991.
32. M. Mokhtaari, *Advanced microwave filter design*, PhD Thesis, University of Victoria, Victoria, Canada, 2008.

BIOGRAPHIES



Marjan Mokhtaari received her B.Sc. and M.Sc. degrees with honors from Sharif University of Technology in Iran in Electrical Engineering and Telecommunications in 1998 and 2000, respectively, and the Ph.D. from the University of Victoria, Victoria, BC, Canada, in 2009. She was

a Senior Research and Microwave Design Engineer in Iran Telecommunication Research Center (ITRC). During graduate studies, she was involved in different projects on advanced microwave filter designs for dual/multi to ultra wide band applications. She also collaborated with some companies and research centers including the Herzberg Institute of Astrophysics (HIA), National Research Council of Canada (NRC-CNRC), Daniels Electronics Ltd. and Comdev as part of an internship program at the University of Victoria. She has been working as a Microwave Research associate at University of Victoria since April 2009. She is interested in advanced designs, development, and measurements of microwave/RF sub-systems and components, antennas, MMIC, computational electromagnetics, inverse scattering, and telecommunications.



Jens Bornemann is currently a Professor at the University of Victoria, Victoria, BC, Canada. From 1992 to 1995, he was a Fellow of the British Columbia Advanced Systems Institute. In 1996, he was a Visiting Scientist at Spar Aerospace Limited (now MDA Space) and a Visiting

Professor at the University of Ulm, Germany. From 1997 to 2002, he was a co-director of the Center for Advanced Materials and Related Technology. From 1999 to 2002, he served as an Associate Editor of the *IEEE Transactions on Microwave Theory and Techniques*. In 2003, he was a Visiting Professor at the Laboratory for Electromagnetic Fields and Microwave Electronics, ETH Zurich, Switzerland. He has authored/coauthored more than 220 technical articles. His research activities include the design of RF/wireless/microwave components and antennas. Dr. Bornemann is a Registered Professional Engineer in the Province of British Columbia, and a Fellow IEEE.



Smain Amari received the DES degree in Physics and Electronics from Constantine University, Constantine, Algeria, in 1985, and the Masters degree in Electrical Engineering and Ph.D. degree in Physics from Washington University, St. Louis, MO, in 1989 and 1994, respectively. From 1994 to 2000, he was in the Department of Electrical and Computer Engineering, University of Victoria, Victoria, BC, Canada. From 1997 to 1999, he was a Visiting Scientist with the Swiss Federal Institute of

Technology, Zurich, Switzerland, and a Visiting Professor in summer 2001. Since November 2000, he has been with the Department of Electrical and Computer Engineering, Royal Military College of Canada, Kingston, ON, Canada, where he is currently a Professor. He is interested in Numerical Analysis, Numerical Techniques in Electromagnetics, Applied Physics, Applied Mathematics, Wireless and Optical Communications, CAD of Microwave Components, and Application of Quantum Field Theory in Quantum Many-Particle Systems.